Biophysical Journal
Article

Biophysical Society

Scavenging amyloid oligomers from neurons with silica nanobowls: Implications for amyloid diseases

Vrinda Sant,[1,*] Madhura Som,[2] Abhijith G. Karkisaval,[3] Parker Carnahan,[4] and Ratnesh Lal[1,3,*]
[1]Materials Science and Engineering, [2]Department of Nanoengineering, [3]Department of Mechanical and Aerospace Engineering, and [4]Department of Bioengineering, University of California San Diego, La Jolla, California

ABSTRACT Amyloid-β (Aβ) oligomers are toxic species implicated in Alzheimer's disease (AD). The prevailing hypothesis implicates a major role of membrane-associated amyloid oligomers in AD pathology. Our silica nanobowls (NB) coated with lipid-polymer have submicromolar affinity for Aβ binding. We demonstrate that NB scavenges distinct fractions of Aβs in a time-resolved manner from amyloid precursor protein-null neuronal cells after incubation with Aβ. At short incubation times in cell culture, NB-Aβ seeds have aggregation kinetics resembling that of extracellular fraction of Aβ, whereas at longer incubation times, NB-Aβ seeds scavenge membrane-associated Aβ. Aβ aggregates can be eluted from NB surfaces by mechanical agitation and appear to retain their aggregation driving domains as seen in seeding aggregation experiments. These results demonstrate that the NB system can be used for time-resolved separation of toxic Aβ species from biological samples for characterization and in diagnostics. Scavenging membrane-associated amyloids using lipid-functionalized NB without chemical manipulation has wide applications in the diagnosis and therapy of AD and other neurodegenerative diseases, cancer, and cardiovascular conditions.

SIGNIFICANCE Amyloid-β protein oligomers are implicated in neurodegenerative disease pathology. Early membrane-associated protein aggregates are the toxic species responsible for dementia and Alzheimer's disease. We report that silica nanobowls tightly adsorb amyloid-β aggregates without altering their native aggregation-driving domains and sequesters amyloids out of the cell membrane. Using nanobowls to scavenge and elute membrane-associated early occurring toxic amyloids from cells and tissues without chemical intervention is uniquely well suited for determining disease-relevant specific therapeutic targets in amyloidosis, such as neurodegenerative diseases, cancer, and cardiovascular conditions.

INTRODUCTION

Amyloid-β (Aβ) fibrils form the major component of extracellular plaques, a hallmark of neurodegenerative diseases like Alzheimer's diseases (AD). These fibrils are the end stage of a dynamic aggregation process, the intermediates of which have been shown to be toxic to neurons manifesting in reducing synapse number, inhibiting long-term potentiation, and impairing memory (1,2). The current paradigm implicates pathological membrane interactions of early Aβ aggregates as a key step in the AD cascade, including enhanced nucleation, membrane disruption, and pore formation (3–7). Nanoparticles (NP) have attracted attention for studying Aβ biochemistry because of their large surface/volume ratio and availability of a wide range of materials that allow for noninvasive actuation of a multitude of functions. NP surfaces are studied as nucleation sites for the formation of disease-relevant species and aggregation modulation (8–13). Chemisorption on anti-Aβ antibody-conjugated nanoparticles and removal of Aβ has also been demonstrated (12,14). The interaction between Aβ oligomers and lipids, especially with anionic interfaces, have been extensively studied (15–17). Additionally, silver NP coated with lipids have been used to study the secondary structure of membrane-attached Aβ oligomers, a much-coveted topic in the AD community (18).

Over the years, considerable effort has been spent on developing models of Aβ oligomers that have been implicated as upstream and early occurring toxic species (19–25). These brain-derived and synthetically prepared aggregates have diverse and heterogenous secondary and quaternary structures, indicating that Aβ pathology is not a result of a single toxic species (26). The diversity of amyloid aggregate morphologies has been linked to phenotypic differences in clinical features of dementia (27), although several species formed

Submitted February 23, 2021, and accepted for publication July 1, 2021.

*Correspondence: vsant@ucsd.edu or rlal@ucsd.edu

Editor: Sudipta Maiti.

https://doi.org/10.1016/j.bpj.2021.07.002

during the aggregation cascade of Aβ in vivo remain unreported. This is, in part, because traditional protein isolation methods use harsh elution conditions like extreme pHs and detergent treatments (23,24), which often disrupt inter- and intra-molecular interactions in weakly held transient amyloid oligomeric species. The inability to isolate a broad spectrum of toxic Aβ species from biological samples has thus stymied therapeutic development for AD and other amyloid diseases.

Our study used silica nanobowls (NB) with lipid-polymer coating (Fig. 1) that present a unique hybrid interface to address the above-mentioned challenge. NB, with high affinity for Aβ, can facilitate isolating transient and soluble Aβ aggregates. We evaluate NB for quantitative estimation of binding kinetics of amyloid oligomers and elucidate the mechanism by which NB scavenge two distinct fractions of extracellular and membrane-associated Aβ in neuronal cultures. NB's high affinity for Aβ can be attributed to silica's negative surface charge, analogous to Aβ's high affinity for anionic vesicles. This is advantageous over antibody-functionalized NB as it offers simplified elution. We demonstrate that Aβ adsorption on NB is reversible and poses a facile method for separation from serum-like environments. Scavenging and eluting early amyloid aggregates with NB have a significant impact in identifying the specific disease-causing species and therapeutic targets for various amyloidosis.

MATERIALS AND METHODS

Tetraethyl orthosilicate, poly(N-isopropylacrylamide), ammonium hydroxide, dimethyl formamide (DMF), fluorescein isothiocyanate (FITC), Tween 20, 3-aminopropyl triethoxy silane (Sigma-Aldrich, St. Louis, MO), Calcein AM (CAM) (MilliporeSigma, Burlington, MA), polystyrene (PS) spheres (PolySciences, Warrington, PA), 1,2-dioleoyl-*sn*-glycero-3-phosphoethanolamine (DOPE), rhodamine-labeled 1-palmitoyl-2-oleoyl-sn-glycero-3-phosphoethanolamine (Rh-PE) (Avanti Polar Lipids, Alabaster, AL), Opti-MEM (OM) reduced serum media, phosphate saline buffer (PBS), Thioflavin T (ThT) (Thermo Fisher Scientific, Waltham, MA), cell culture slides (MatTek, Ashland, MA), Aβ peptide (AnaSpec, Fremont, CA), biotinylated Aβ antibody (Mabtech, Stockholm, Sweden), MTT (3-(4,5-dimethylthiazol-2-yl)-2,5-diphenyltetrazolium bromide) (Abcam, Cambridge, UK), and Cell Fractionation Kit by Cell Signaling Technology (Danvers, MA) were used.

Nanoparticle synthesis, payload encapsulation, and payload quantification

Synthesis of NB

NB were synthesized as described previously (28). Briefly, 55 μL tetraethyl orthosilicate and 100 μL PS spheres (100 nm, COOH modified) were added

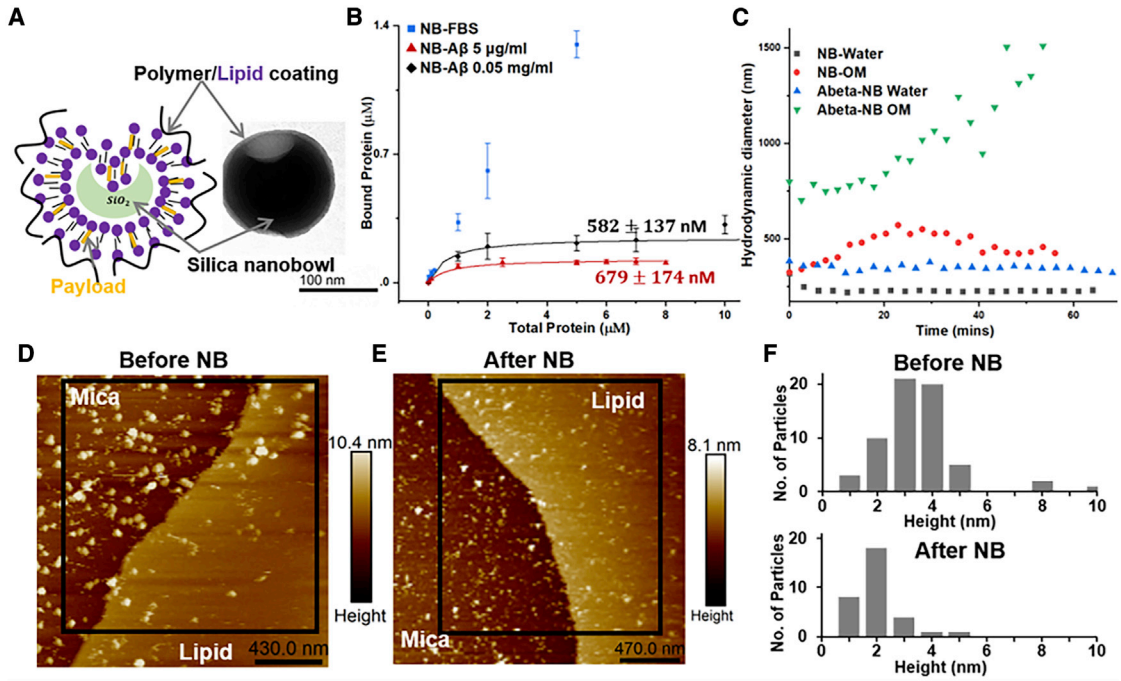

FIGURE 1 (*A*) Silica NB schematic and morphology. Left: schematic. Right: TEM image showing a coating halo encapsulating a dense silica NB. The hydrodynamic diameter and stability of NB are shown in Fig. S1. (*B*) Binding saturation of Aβ with 0.05 mg/mL (*black diamonds*) and 5 μg/mL (*red triangles*) NB fitted to the Hill model (*lines*) for Kd determination. Kd for serum proteins (FBS: fetal bovine serum) is not calculated as it does not saturate. Error bars represent SDs from three independent measurements. Kd is 582 $\pm$ 137 nM at 0.05 mg/mL NB and 679 $\pm$ 174 nM for 5 μg/mL NB. These are within one SD of each other. (*C*) Kinetic hydrodynamic diameter for dynamic NB and Aβ interactions from DLS. Experiments were performed in water and reduced serum cell culture media Opti-MEM (OM). (*D* and *E*) The effect of NB addition on AFM images of Aβ-reconstituted DOPC (phophocholine) bilayers. Images show a section of mica on the left and supported lipid bilayers (SLB) on the right. After forming the supported lipid bilayers on mica (*D*), NB were added, incubated for 10 min, and washed before the sample was imaged again (*E*). (*F*) The height distribution of Aβ oligomers analyzed for each image in the area is indicated by the black box in (*D*) and (*E*). The number of particles have been binned from integer-to-integer height value. A shift in average oligomer heights from 3–4 to 2 nm is observed after NB treatment. 62 particles were counted for (*D*) and 32 for (*E*). To see this figure in color, go online.

together in a stirring solution of 1.3 mL NH_4OH (28% aqueous), 4 mL isopropyl alcohol, and 0.7 mL deionized (DI) water. The solution was stirred at room temperature for 2 h, and 200–300 nm silica-PS Janus templates were isolated by centrifugation. The mixture was first centrifuged at 500 rcf for 5 min. The supernatant from the first spin was isolated and centrifuged again at 3200 rcf for 5 min and washed in 200 proof ethanol. To achieve NB, the PS core was solubilized by suspending silica-PS cores in ~6 mL DMF and stirring at 60°C overnight. DMF was removed by centrifuging at 3200 rcf for 5 min and washing pellet in ethanol three times. Yield was determined by drying NB and weighing them in a glass vial.

CAM encapsulation

For encapsulation, a mixture of lipid (DOPE) and polymer (p-NIPAM, Poly(N-isopropylacrylamide)) was used. DOPE (10 mg/mL) and p-NIPAM (3 mg/mL) stock solutions were prepared in chloroform. CAM was used as the payload in this study. CAM 0.2 mg/mL stock was prepared in chloroform. Payload (CAM 4 μL) was dried under vacuum with DOPE (0.25 mL) and p-NIPAM (0.417 mL) overnight. The next day, dried lipids/polymer/payload were suspended in 5 mL DI water and sonicated in a water bath for 15 min.

Dried NB were resuspended in DI water to a concentration of 1.56 mg/mL by brief sonication (5–15 min). 0.75 mL of NB were added to the payload-lipid mixture and sonicated on ice with a probe sonicator (70% power, 20 kHz, 90 s). The mixture was then stirred overnight. Lipid-polymer-containing payload deposits on the silica surface as supported multilayers. To separate undeposited lipid-polymer from loaded NB, the mixture is centrifuged once at 3200 rcf for 5 min. The pellet is resuspended in water to the desired concentration. Loaded NB were used within 3 days of preparation and stored at 4°C for this duration. Size was measured by dynamic light scattering (DLS) on Malvern Zetasizer (Malvern Panalytical, Malvern, UK). Morphology was confirmed by transmission electron microscopy (TEM) on FEI Tecnai Spirit G2 BioTWIN TEM.

Loaded and coated NB were stable for 3 days on storage in 4°C (ζ-potential and DLS measurements). For each experiment, fresh NB were prepared and used within 3 days.

Delivery of payload to B103 cells: uptake of CAM

The said concentration of NB carrying CAM was introduced to cells in OM in 96-well plates. Fluorescence was recorded every 15 min on a spectrometer at excitation/emission 485/520 nm. The temperature was maintained at 37°C for all experiments unless otherwise mentioned. For uptake with Aβ, cells were incubated with Aβ for 6 h, then NB carrying CAM were added to media, and fluorescence reading was collected. Nonfluorescent CAM dissociates to fluorescent CA after cleavage by transmembrane esterases.

Exogenous Aβ incubation and subsequent treatment

Cells were plated in tissue culture-treated 96-well plates the night before peptide addition. The next day, Aβ was added to a concentration of 5 μM in OM (or for controls, peptide suspension buffer), unless otherwise mentioned. After 6 h, the media was decanted and treated with control (buffer) or NB at 0.05 mg/mL NB (unless otherwise mentioned) in OM. After an additional 17 h, media was decanted, and other detection assays were conducted.

Immunostaining, confocal laser scanning microscopy, and image analysis

SP8 Leica confocal microscope (Leica Microsystems, Wetzlar, Germany) was used to obtain images at 100× magnification. Cells were grown on a No. 1.5 coverglass cell culture dish coated with poly-D-lysine (MatTek) at a seeding density of 2×10^5 cells/mL. After said treatment and duration, cells were washed with PBS and fixed with 4% paraformaldehyde in PBS. They were either imaged directly after fixing in the case of labeled NB or postimmunostaining. For Rh-PE, the dsRED line was used with excitation/emission at 558/583 nm on a 100× objective. For immunostained Aβ, the FITC line was used. Generally, the total depth of fixed cells from the coverslip was 10.73–11.04 μm. On average, images were captured in a plane that was 6–8 μm from the top of the coverslip.

Immunostaining was carried out after fixing cells. Cells were then blocked for 30 min in 1% bovine serum albumin and 22.52 mg/mL glycine in PBS + 0.1% Tween-20 (PBST). After decanting, cells were incubated with 2:5000 dilution (in 1% BSA in PBST) of biotinylated mAb and bm-AβN for 1 h. After washing with PBS, cells were incubated with 0.025 mg/mL streptavidin-FITC (in PBST; BioLegend, San Diego, CA) for 45 min, washed with PBS three times, and stored at 4°C until imaging. A permeabilization step was not performed as that seemed to destroy the membrane and give much smaller yield. However, because antibody dilution buffer contains Tween-20, imaging intracellular Aβ was still possible.

Cytotoxicity MTT assay

After peptide incubation and treatment, 50 μL of media was removed from each well, and 10 μL/well of warmed MTT (12 mM in PBS) was added. After incubating at 37°C for 4 h, 85 μL of supernate was replaced with 100 μL of DMSO/well. After a 10-min incubation at 37°C, an absorbance reading was taken at 540 nm. For samples that were treated with NB, an absorbance reading higher than the control (no Aβ, no treatment) was often obtained. This is because formazan shows higher absorbance with NB in a concentration-dependent manner. It was accounted for by setting the maximal possible viability to 100%, as defined by the negative control, if a larger value was obtained. Absorbance for all samples in each experiment was normalized to the control. Often, MTT assay was performed with the same samples that were used for dye leakage assay, enabling facile correlation between data. In this case, CA measurements for dye leakage were done before the MTT addition. All data have been normalized to the absorbance of the cells in which no Aβ or NB are applied.

In situ dye leakage assay

This assay works on the principle of measuring the fluorescence of CAM retained in cells over time. For this, CAM (stock prepared in DMSO) was added to cells in a 96-well plate to a final concentration of 1 μg/mL and incubated at 37°C for 30 min. Some amount of CAM enters cells spontaneously and is cleaved to fluorescent CA. CAM that has not entered cells is removed by decanting and replaced with fresh media. At this point, fluorescence of CA was measured at time t = X. Over time, CA will either diffuse out of cells passively or because of impaired membrane integrity. After Y hours, media was replaced, removing all CA that leaked out of cells, and fluorescence was measured again. The percentage difference in fluorescence between t = X and t = Y as a ratio of fluorescence at t = X is presented here. Each experiment consisted of three repeats, and the experiments were repeated three times. Results are presented as the weighted average of the percentage difference from all experiments and the corresponding mean ± SE.

Methods for cell culture, peptide preparation, NB, lipid and Aβ quantification, image processing, and dissociation constant (Kd) measurements are found in the Supporting materials and methods.

RESULTS

Silica NB have high affinity for $A\beta_{1-42}$

Silica NB are composed of a silica core coated with a lipid-polymer coating. DOPE is used as the lipid and polymer is p-NIPAM. In Fig. 1, a halo around a dark core (silica) in a

TEM image represents the coating. The lipid serves as a hydrophobic environment for carrying a small molecule payload like an intracellular dye probe or therapeutic molecule. The hollow pit in the silica core increases the surface area for carrying capacity. The lipid-polymer coating prevents nonspecific protein adsorption (29,30).

The Kd of NB and Aβ was measured using a bulk method wherein the NP bound and unbound fractions of Aβ were separated and concentration quantified by the Bradford assay. The same measurement was also done for serum proteins from calf serum. Calf serum protein binding to NB does not saturate in the range measured, indicating that they are constantly adsorbing and desorbing from the NP surface, conferring no specific affinity, as seen in the DLS measurements (Fig. 1 *C*). On the other hand, Aβ binding appears to saturate at 0.2 μM and can be fit to the Hill model to determine a Kd of $\sim$600 nM (Fig. 1 *B*). Before separation and protein quantification, a freshly prepared solution of Aβ are incubated at 37°C for 40 min; DLS measurements indicate that this is the amount of time for stabilization of peptide-particle interactions (Fig. 1 *C*). For similar preparations of Aβ, we have shown that a fresh solution consists primarily of monomers, 3-mers, 4-mers, and 5-mers (31). DLS measurements indicate that in buffer, Aβ quickly adsorbs onto the NB, on a timescale smaller than the time taken for the first measurement (Fig. 1 *C*). Once a 100-nm layer of the protein forms, it remains consistently adhered on NB, without fluctuations. In contrast, when serum proteins are present in solution, DLS measurements show agglomeration of NB that would result in sedimentation. Aβ-reconstituted supported bilayers were imaged on an atomic force microscope (AFM) before and after NB treatment (Fig. 1, *D* and *E*). The Aβ oligomer height distribution undergoes drastic shift from a peak at 3–4 to 2 nm after NB treatment (Fig. 1 *F*).

Characterizing B103 cells and Aβ interactions

MTT assay was used as an indicator of toxicity of Aβ when applied to B103 cells. First, a concentration-dependence assay on Aβ incubation overnight showed that mitochondrial metabolism was reduced to 60 and 80% for 5 and 10 μM of Aβ, respectively, as opposed to 20 μM Aβ, in which no difference was seen. The high concentration does not show any detectable reduction in MTT absorbance from control (Fig. 2 *A*), suggesting that Aβ leads to cell toxicity in a concentration-dependent manner. Higher concentrations fibrillate Aβ almost immediately in cell culture media as shown by kinetic ThT measurements (Fig. 2 *B*). Aβ in cell culture media at 5 μM has a substantial lag phase of $\sim$3–6 h, even in the presence of a relatively high concentration of lipids (0.2 mg/mL as compared with the estimated lipid concentration for MTT experiment 5.4 ng/mL), allowing prolonged oligomer-cell interactions.

Next, we conducted time-dependent MTT and dye leakage assays. One of the most widely studied pathways

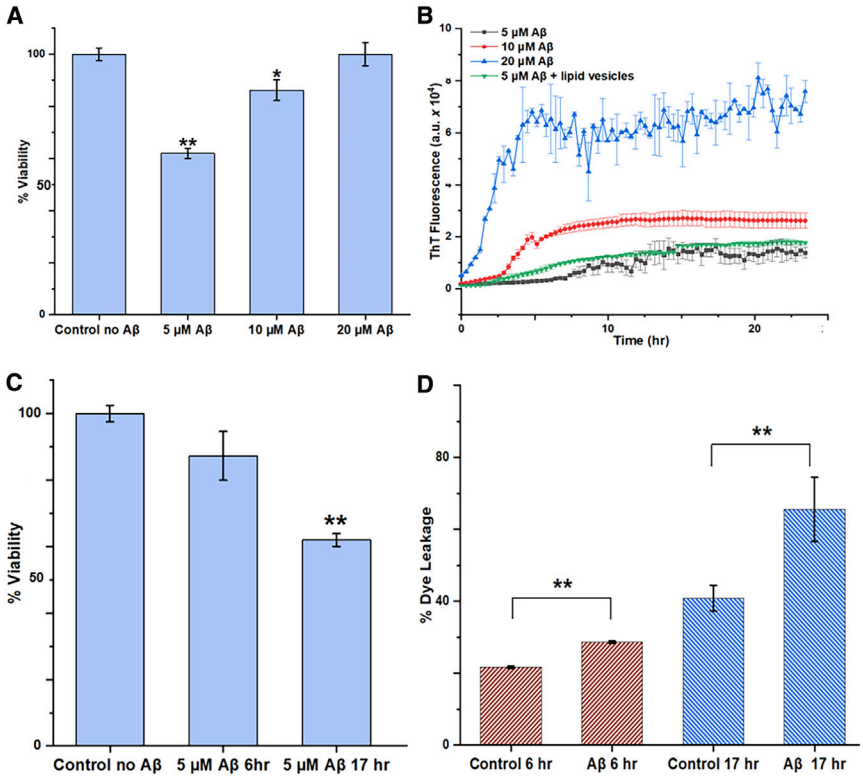

FIGURE 2 Aβ pathology in B103 cells. (*A*) Cell viability from MTT assay. Absorbance was normalized to control cells without Aβ. Error bars represent mean $\pm$ SE from at least three repeats. Significance from *t*-test: $^{**}p < 0.001$ and $^{*}p < 0.02$. (*B*) ThT kinetic assay for Aβ in OM. Vesicle concentration is 0.2 mg/mL made of DOPS/POPE (phophocholine/ phosphoethanolamine) (1:1). Results are mean $\pm$ SE from three repeats. (*C*) Time-dependent cell viability from MTT assay. Results represent mean $\pm$ SE from at least three repeats. $^{**}p < 0.001$. (*D*) CA dye leakage representing membrane disruption for application of 5 μM Aβ. The *y* axis represents the weighted average of 8–10 independent samples, and results correspond to mean $\pm$ SE. Statistical significance was analyzed using an unpaired *t*-test. $^{*}p < 0.02$ and $^{**}p < 0.001$. To see this figure in color, go online.

for the toxicity of intermediates are their pathological cell membrane interactions—pore formation, lipid sequestering, and membrane thinning, leading to membrane disruption (5,25). The effects of membrane disruption are visible in the dye leakage assay using CAM, a membrane-permeable fluorescent small molecule. CAM is a small molecule and often diffuses passively from cells (32). Thus, all dye leakage data were interpreted relative to its passive leakage: 20% at 6 h and 40% at 17 h. At 6 h after incubation with Aβ, no significant difference in MTT absorbance was observed (Fig. 2 *C*). In contrast, the cell stress induced by 5 μM Aβ increased the leakage of small molecules from membranes from 20 to 40% ∼6 h after incubation (Fig. 2 D). Dye leakage is increased to ∼70% over the next 17 h, and the concomitant cell death is observed because of irreversible cell membrane and cell damage.

Spatial localization of exogenously added Aβ was determined by immunostaining with anti-Aβ antibody. Image analysis across the central plane of cells (edges of cells are cell membranes; the central void is the cytoplasm with nucleus) showed that aggregates are primarily located at the periphery of cells and neurites; no detectable intracellular Aβ is observed (Fig. 3, *B* and *C*). Shift of size distribution of aggregates to larger than 1 μm^2 suggests the formation of higher order assemblies (Fig. 3 *F*). The intensity/cell estimates the amount of Aβ-associating to cells (Fig. 3 *E*). 6 and 11 h have similar intensity/cell, indicating that Aβ does not degrade for the duration of the experiment.

The amount of Aβ and membrane-associated Aβ was quantified using ThT assay in cell lysate and decanted cell media from cell culture (Table 1). Traditional methods like Western blots and ELISA may give more precise information (the mean ± SE for some of these measurements are very large). However, ThT aggregation assays are often used for diagnostics to quantify amyloid in tissue samples and cerebrospinal fluid (33); they are sometimes more sensitive and yield results faster than the above-mentioned bioassays (34). After 6 h, the amount of Aβ that remained associated with cells was highly dependent on cell density contributing to large errors in the ThT assay. The amount dissociated from cells by decanting was ∼25% of the initial 5 μM as found from ThT quantification. About ∼70% remains strongly associated with cells, amounting to a true concentration responsible for the toxicity of ∼3.75 μM. In an experiment, after Aβ incubation was started, cell culture media was repeatedly changed over the course of time. In each change, the amount of Aβ in the decanted fraction was quantified. It was found that ∼20–30% Aβ was always

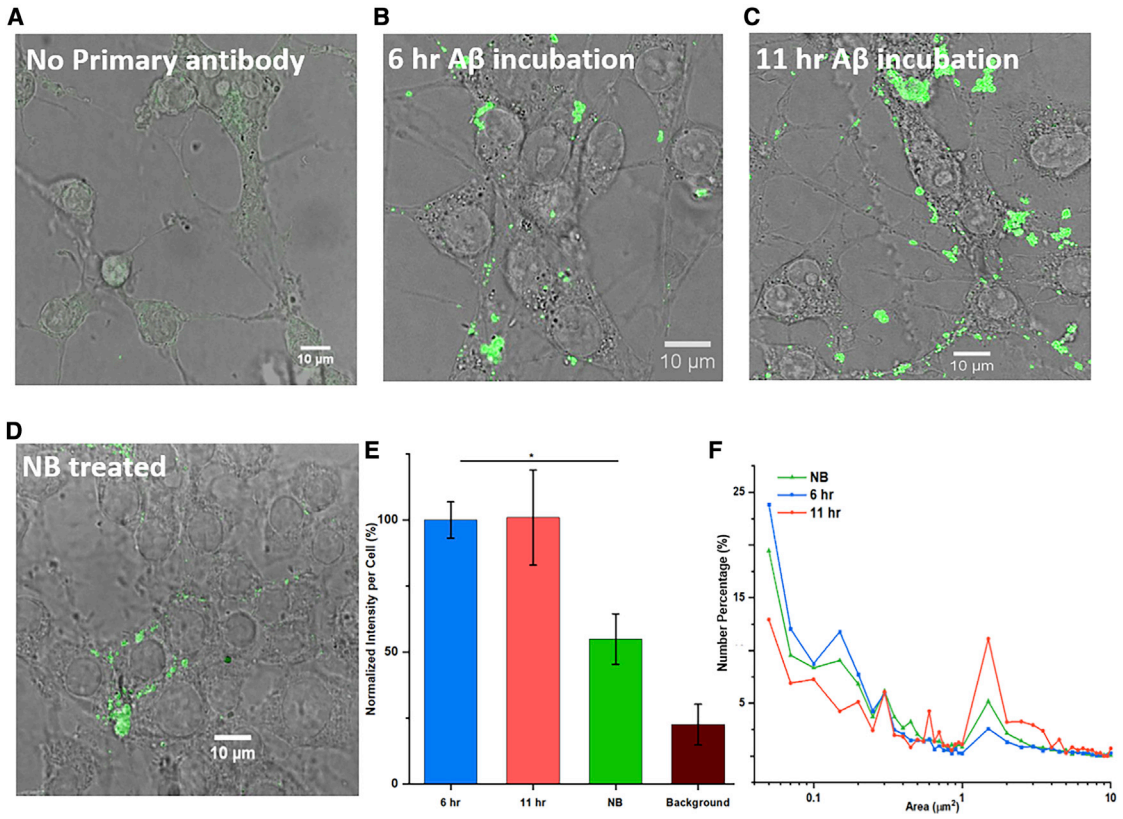

FIGURE 3 Representative images from immunostaining for Aβ after (*A*) no primary antibody or Aβ, (*B*) 6 h Aβ incubation, (*C*) 11 h Aβ incubation, (*D*) 6 h Aβ incubation and 17 h 0.05 mg/mL NB application. (*E*) Intensity per cell found by image analysis on ImageJ. Error bars represent SDs from six images from two independent experiments. Statistical significance was determined from a *t*-test with $*p < 0.05$. (*F*) Size distribution of Aβ aggregates. To see this figure in color, go online.

TABLE 1 Proportion of Aβ in cell lysates compared with those adsorbed on NB

	Removed at 360 min (% Total)	Cell Culture Supernate at 390 min (% Associated with Cell)	Cell Culture Supernate at 17 h (% Associated with Cell)	In Cell lysate at 17 h (% Associated with Cell)
Aβ	21.96 (3.03)	26.78 (2.11)	32.30 (16.58)	88.07 (12.83)*
Aβ w/NB	20.12 (4.46)	50.94 (2.29)	75.95 (15.64)	45.40 (5.97)*

Aβ was exogenously added to cell cultures at 5 μM. After 360 min of incubation, any Aβ that had not bound to cells was decanted (column 2). After an additional 30 min (390 min from the beginning), the decanted supernate was measured again (column 4). This time point was chosen primarily to probe the equilibrium between cell-bound and soluble Aβ. 17 h after the previous time point, the cell supernate and lysate was collected for Aβ quantification (column 4 and 5). Results are mean $\pm$ SE from three repeats. SE is presented in parenthesis.
*$p < 0.05$ from Student's *t*-test.

present in the cell media as a soluble fraction or weakly adhered to cell membranes (Table 1). In the following text, we will refer to the fraction of Aβ recovered from decanting cell culture media as "extracellular" and the fraction found in cell lysates (ecAβ), the source of which is likely to be cell membrane bound, inserted, or electrostatically adsorbed, as "membrane associated," (mAβ).

Membrane-associated Aβ depleted after application of silica NB

Silica NB were added to cells in fresh media after decanting soluble Aβ 6 h postincubation. This time point of application was chosen because, although Aβ showed pathological activity in the dye leakage assay, no significant cell death was observed during this time period. Media was decanted 30 min and 17 h after NB were applied for soluble Aβ quantification; immunostaining for Aβ was conducted at 17 h. Remarkably, analysis of immunostained images showed half the initial (6 h) amount of Aβ after application of NB results (Fig. 3 *E*).

We hypothesized that the remaining membrane-associated Aβ could have two fates: 1) application of NB overstimulates autophagy and, consequently, the cell overexpresses Aβ-degrading enzymes, thereby accelerating its degradation. In this case, application of NB in B103 cells would result in an increased amount of secreted protein. Bicinchoninic acid assay was used to quantify protein in decanted media and trypsinized extracellular matrix for cells incubated with NB. No significant difference in the secreted protein was found as compared with when no NB were applied (Fig. S2 *B*), suggesting that NB do not accelerate Aβ degradation. This is consistent with previously reported findings on autophagic response induced by nanoparticles (35). 2) The second possibility was that the "disappeared" Aβ is adsorbed onto the NB surface. In this case, the remaining Aβ should be retrieved in cell media that was decanted before fixing. This hypothesis is supported with the quantification of NB-adsorbed Aβ by ThT after NB application. NB-associated Aβ 30 min after application accounts for $\sim$50% of Aβ; this fraction increases to $\sim$76% after 17 h (Table 1). If extracellular and membrane-bound Aβ form fibrils of distinct ThT binding capability, ThT quantification of Aβ concentrations would not be accurate. To address this concern, we obtained a calibration curve for ThT fluorescence and Aβ concentrations by aggregating different concentrations of Aβ in cell lysate. This will also compensate for fibril polymorphism if it occurs in this experimental system. As such, we relied upon ThT measurements to support our hypothesis that Aβ is depleted from neuronal membranes in the presence of NB; this is primarily supported by Kd measurements (Fig. 1 *B*) that show affinity for Aβ and immunostaining of Aβ in neuronal cultures.

NB application alleviates cell from Aβ pathology

MTT assay was used to assess the toxicity of NB in healthy B103 cells. At the NB concentrations tested, 5 μg/mL and 0.05 and 0.5 mg/mL, no significant impairment to mitochondrial metabolic activity or membrane leakiness was found for 17 h of incubation (Fig. S2, *C* and *D*). NB were applied to cells incubated with Aβ that showed impaired membrane leakiness at 6 h. NB at all concentrations showed significantly improved mitochondrial metabolic activity than the control (cells incubated with Aβ for 24 h without the application of NB) (Fig. 4, *A* and *B*). Similarly, membrane leakiness from these impacted cells was also recovered to the same level as healthy cells (40%). The possibility that the therapeutic effect occurs because of modulation of Aβ aggregation dynamics is ruled out as NB do not affect the ThT kinetics of Aβ at concentrations used in the study (Fig. S2 *A*).

Reversibility of NB adsorption of Aβ and its seeding capability

We anticipated that the association of Aβ and NB would be reversible because it is driven by adsorption rather than antibody recognition. To test this hypothesis, pellets with bound Aβ and NB were resuspended, vortexed, and quantified following the steps in Fig. S3. Vortexing applies strong shear forces to mechanically detach the adsorbed protein from the NB surface rather than chemical intervention. All of the initially bound protein was found in the supernatant, confirming the reversibility of the process (Fig. 5 *B*). Additionally, we have preliminary measurements to show that during the isolation process, after the first centrifugation step (Fig. S3), the total amount of NB-bound protein is

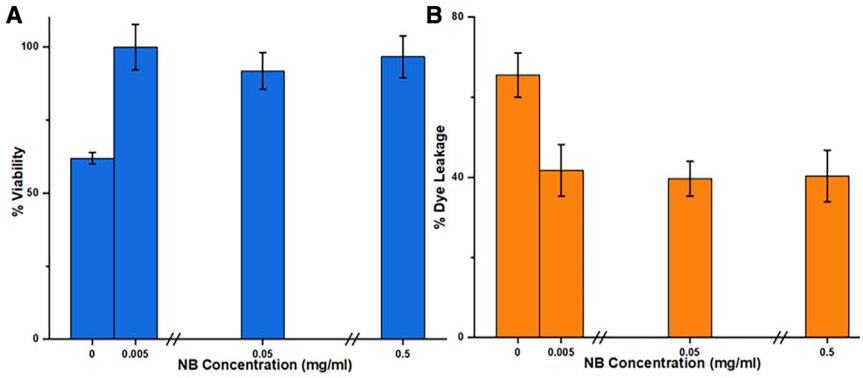

FIGURE 4 Depletion of Aβ and mitigation of its pathology in B103 cells. (*A*) Cell viability from MTT assay and (*B*) dye leakage at 17 h for cells when NB are applied 6 h postincubation with Aβ. Cells incubated with Aβ for 17 h have reduced cell viability at 60% and increased dye leakage at 70%. Applying NB to cells with Aβ prevents cell death and restores dye leakage to ~40%, like that of "healthy" cells (untreated with NB or Aβ). Results represent mean ± SE for data collected from at least three independent experiments with three to eight samples for each condition. To see this figure in color, go online.

very close to NB-Aβ (Table S1). This finding suggests that during the isolation process, nonspecific protein adsorption on NB is efficiently minimized by dilution and centrifugation.

ThT kinetic curves collected to determine Aβ concentration are essentially seeding experiments wherein seeds from cell culture fractions are mixed with monomer for amplification. As such, ThT kinetics hold key information on the nucleating and elongation properties of these Aβ fractions. For this, the kinetic plots were fit to equations previously proposed to describe amyloid sigmoidal aggregation (36,37), and parameters, time to half maxima ($T_{1/2}$) and

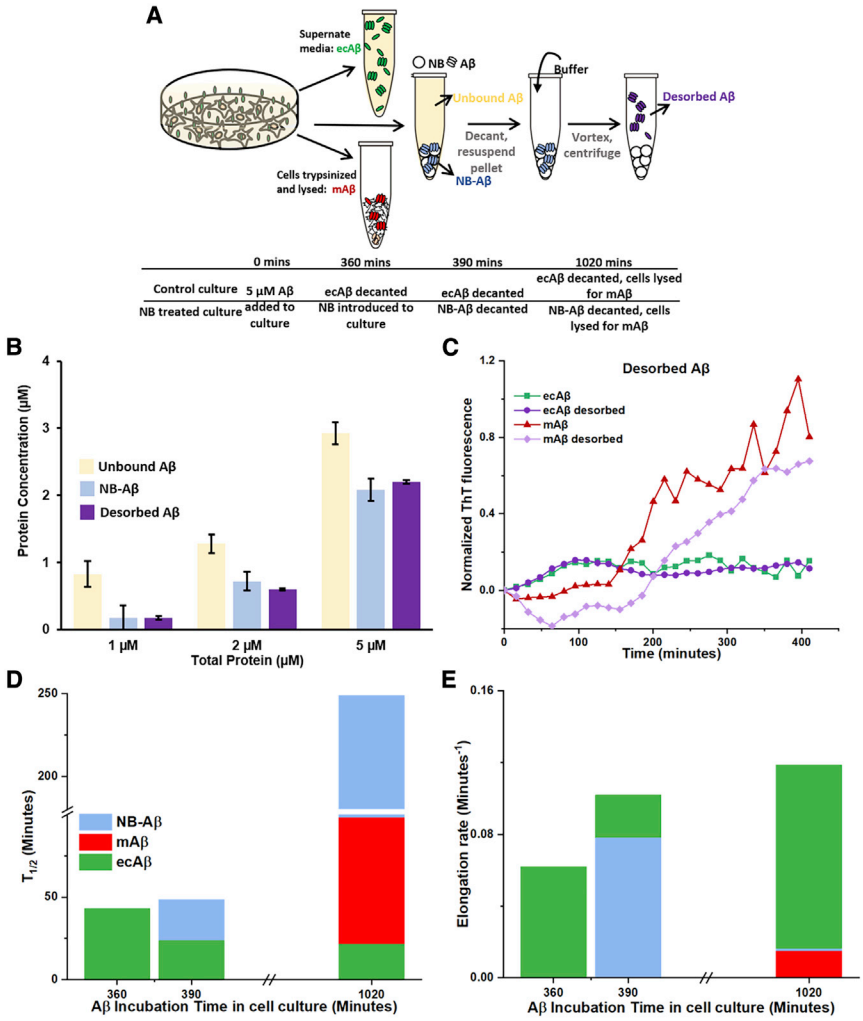

FIGURE 5 Reversibility of NB adsorption. (*A*) (*Top*) Schematic showing how samples are isolated and processed. (*Bottom*) Timeline illustrating when ecAβ, mAβ, and NB-Aβ are collected for seeding experiments (*C–E*). (*B*) Aβ and NB are incubated in buffer overnight at 37°C. NB-adsorbed Aβ is separated by centrifugation and concentration measured by Bradford assay as seen on the schematic on the right. The concentration of the solution is measured again after vortexing, centrifuging, and decanting desorbed protein as shown in Fig. S6. For all concentrations measured, NB-bound protein is desorbed after vortexing. Results are mean ± SE from three repeats. (*C*) Similarity in aggregation behavior of Aβ desorbed from NB at different Aβ incubation times in cell culture. The curves are normalized to the saturation value of maximal possible amount of protein (12 μM) in culturing media without Aβ or NB. Curves are averages from three repeats. (*D* and *E*) Time to reach half maxima and elongation rate from fitting of ThT curves for seeds of given concentration isolated from cell culture at selected time points during incubation. Curves, fitting parameters, and SDs can be found in Fig. S5. (*D*) and (*E*) follow the same legend. To see this figure in color, go online.

elongation rate, were compared. We can establish distinct characteristic aggregation behavior for ecAβ and mAβ. A substantially longer lag phase and slower elongation rate is seen for mAβ in cell lysates (Fig. 5, *D* and *E*; Fig. S8 *D*) than ecAβ. Despite having almost four times the amount of Aβ and a lipid environment known to accelerate aggregation, mAβ in cell lysates show longer $T_{1/2}$ than the ecAβ (Fig. 5 *D*). Poor seeding efficiency of mAβ reinforces studies in which both ex situ and brain-derived toxic Aβ oligomers have been demonstrated as off-pathway to amyloidogenesis (25,38,39). mAβ forms fibrils, even though it exhibits a longer lag phase (Fig. S5 *E*), suggesting that it is off-pathway. A similar phenomenon was seen for off-pathway oligomers by Watanabe-Nakayama et al. (39) in which both on- and off-pathway oligomers aggregate into fibrillar structures.

In our study, none of the extracted fractions show an initial ThT signal different from the background signal. Additionally, the large size distribution of Aβ aggregates seen in microscopy images (Fig. 3 *F*) suggest that ecAβ and mAβ fractions consist of prefibrillar aggregates. Having established a fingerprint for the two Aβ fractions in the experiment, we could infer convincingly that at 390 min, NB-Aβ show $T_{1/2}$ and elongation rate characteristic of ecAβ (Fig. 5, *D* and *E*). After longer incubation, the aggregation parameters shift toward behavior exhibited by mAβ. As NB do not appear to have a major influence on aggregation kinetics in OM, the difference in aggregation kinetics over time could be attributed to the adsorption of the distinct species, respectively (Fig. S2 *A*). Desorbed NB-Aβ show kinetic trends and saturation fluorescence units comparable to samples before vortexing (Fig. 5 *C*).

Preliminary mechanism of Aβ scavenging by NB

At maximum, only ~10% of NB are strongly associated with cells—either anchored to membranes or endocytosed (Table 2). Most NB are found in the supernate decanted from cell culture. However, almost all the labeled lipids are delivered to the cell as 96% are found in the cell lysate (Table 2). This indicates two possible pathways by which NB interact with cells: because of Brownian motion, when NB collide with the cell membrane, they are either endocytosed (4.5% with and 9% without Aβ, Table 2) or they shed their lipid layer on the cell membrane. Fig. 6 *A* shows that at short timescales, lipids on NB cluster on cell membranes, after which they slowly fuse with the cell membrane and other membrane organelles. Consistent with this, Fig. 6 *B* shows an initial rapid rate of intracellular incorporation of CAM, corresponding to lipid clustering. CAM is a dye housed in the lipid coating used to probe intracellular uptake. Lipids in the coating slowly diffuse with the plasma membrane and other membrane-bound intracellular organelles (Fig. 6 *D*).

The fate of the ~90% of the NB in the extracellular media now determines how Aβ is being scavenged. There is strong evidence in literature that Aβ has electrostatic interaction with anionic surfaces (for example, negatively charged lipids and silica) (15–17,40) and weaker interactions with neutral surfaces (16,41). We have demonstrated Aβ's interaction with silica by incubating bare silica NP (no coating) with the protein in solution (Fig. S4). During lag phase, a layer of amorphous aggregates is seen on NP (*top panel*), whereas after longer incubations, NB agglomerate and show fibrillar structures, a finding consistent with published work (15). We believe that the shedding of the lipids is the rate-limiting step for the Aβ-sequestering process by NB, and this also reflects in the observation that payload

TABLE 2 Proportion of labeled NB and lipid in cell lysates compared with those dissociated from the cell

	Cell Culture Supernate at 17 h (% Total)	In Cell Lysate at 17 h (% Total)
NB- cells w/Aβ	95.50 (1.47)	4.50 (0.08)**
NB- cells w/o Aβ	90.95 (1.34)	9.05 (0.18)**
Lipids in NB coating - cells w/Aβ	3.48 (0.005)	96.52 (3.67)
Lipids in NB coating - cells w/o Aβ	4.10 (0.003)	95.91 (4.36)

Results are mean ± SE from three repeats. SE is presented in parenthesis. **$p < 0.005$ in Student's *t*-test.

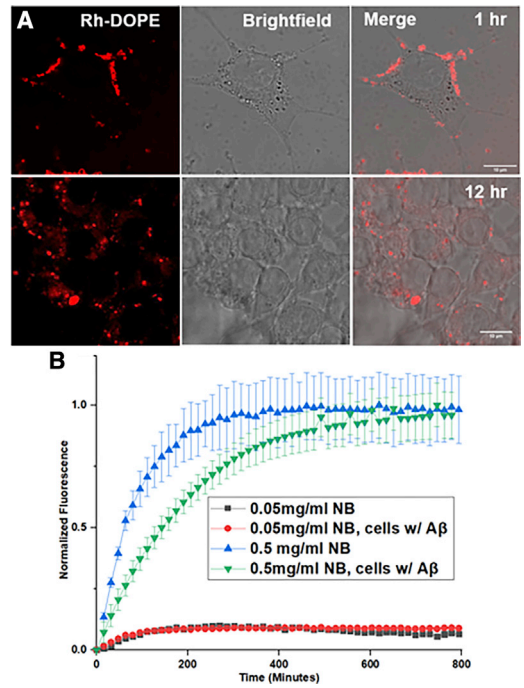

FIGURE 6 (*A*) Confocal laser scanning microscopy images of B103 cells incubated with unloaded 0.05 mg/mL NB labeled with Rh-PE for (*top*) 1 h and (*bottom*) 12 h. (*B*) Payload delivery kinetics in cells with Aβ by uptake and conversion of CAM. Normalized to maximum of 0.5 mg/mL NB signal, and results are mean ± SE from three repeats. To see this figure in color, go online.

incorporation and lipid-cell membrane fusion are unaffected by the presence or absence of Aβ (Table 2).

To account for our findings, we propose a mechanistic pathway (Fig. 7) for Aβ scavenging. Once the NBs shed the lipids, the NB surface picks up Aβ from extracellular media. This is supported by ThT seeding measurements. The elongation rate and $T_{1/2}$ of NB-Aβ collected 30 min after incubation mirrors that of ecAβ (Fig. 5, *D* and *E*). However, NB-Aβ isolated at later time points shows a longer lag phase and slower elongation rates, characteristic of mAβ. As the ecAβ gets sequestered by NB outside the cell, redistribution of mAβ also simultaneously starts trying to reestablish equilibrium of Aβ between the solution and membrane phase. This yields more Aβ to associate with the NB surface over time. The scavenging process is likely to continue until there is equilibrium between the three phases of Aβ (mAβ, ecAβ, and NB-Aβ) or when the NB surface availability has depleted, which depends on NB concentration and size.

DISCUSSION

Silica NP have high affinity for Aβ and scavenge it from cell membranes

We show that silica NB have affinity for Aβ with a Kd of ~600 nM. For therapeutic applications, it is imperative that NB show specificity to Aβ. From DLS and bulk protein measurements (Fig. 1, *B* and *C*), NB appears to bind to serum proteins in fetal bovine serum as well as, to some extent, to proteins in cell culturing media (OM). Fluctuation in the DLS curve indicates that serum protein binding might be dynamic, constantly adsorbing and desorbing. Although NB show proclivity for nonspecific binding to serum proteins in a test tube, a stark difference is observed in neuronal cultures. After separation and centrifugation from neuronal cultures, the total amount of protein bound to NB (as measured by Bradford assay) is the same as the amount of Aβ bound to NB (measured by ThT) (Table S1). This finding indicates a preferential and high affinity interaction between NB and Aβ aggregates.

The dynamics of Aβ between NB and cell membranes are evaluated by comparing Kd for cell membranes. For parallel preparations of Aβ, Kd for synthetic membranes are available in literature. If Aβ displays a similar range for neuronal plasma membranes (520–1200 nM for Dipalmitoylphosphatidylcholine (DMPC)-ganglioside vesicles (42,43)), Aβ would have comparable affinity, if not higher, for NB than for membranes. This suggests that depending on the membrane composition, Aβ would either be in equilibrium with NB-bound and membrane-associated states or preferentially adsorb on NB. The tendency of Aβ to adsorb on NB as implied from Kd analysis would explain the observation that NB application reduces the amount of intensity/cell of mAβ (Fig. 3 *E*). Combining this observation with the mitigation of Aβ pathology upon NB application (Fig. 4 *D*; Table 1), we hypothesize that recovery occurs by the removal of toxic Aβ species. Thus, NB would have therapeutic value for diseases in which Aβ pathology is implicated like cerebral amyloid angiopathy, cardiovascular diseases, and cancer. Additionally, the silica surface of NBs serves as a diverse surface for conjugating different biomolecules like cDNA and antibodies, and the lipid coating can carry small molecules, as we have shown with CAM (44,45). The lipid-polymer coating has been previously shown to prevent nonspecific protein adsorption (29). These additional functionalities would allow the use of NB as therapeutics.

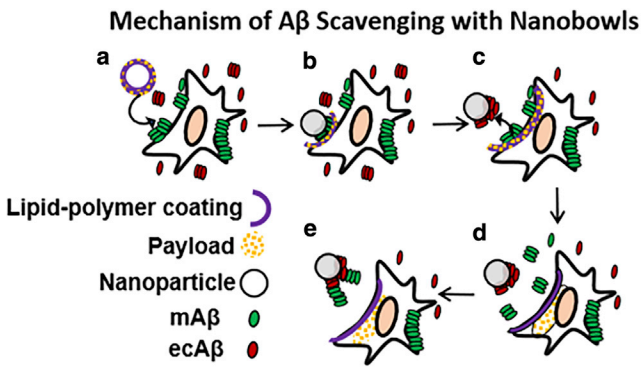

FIGURE 7 Preliminary mechanism of Aβ sequestering with NB. (*a*) NB encapsulating a payload in their lipid-polymer coating collide with cell membranes because of Brownian motion. (*b*) After collision, the lipid-polymer coating adheres to cell, whereas NB diffuse back into solution (~90% of NB). Because the net payload delivery is unaffected by the presence of Aβ (Fig. 6 *B*), we postulate that lipid-polymer coating adhering to the cell membrane and subsequent shedding from NB surface is an upstream rate-limiting step. After NB diffuse back into solution, they adsorb the soluble fraction of Aβ (ecAβ) as the anionic surface of silica is exposed after shedding lipids (*c*). As the soluble pool of Aβ is depleted, mAβ redistributes to solution to re-equilibrate (*d*). The redistributed pool of mAβ then adsorbs on NB, and the process is sequentially repeated (*e*). This leads to sedimentation in stagnant fluid (*e*) as supported by DLS measurements showing formation of 8–10 NB clusters in the presence of Aβ and cell culture media (Fig. 1 *D*). To see this figure in color, go online.

Anionic NB surface enables high affinity for Aβ and its specificity

Aβ adsorbs to a larger extent on vesicles of anionic phospholipids than zwitterionic lipids. Kremer et al. (46) report 50–100% greater mass absorbance of Aβ on POPG (phosphoglycerol) vesicles than neutral POPC (phosphocholine) vesicles. Silica NB share several characteristics with negatively charged vesicles, and we posit that analogous factors affect Aβs adsorption on NB. Aβ and anionic lipid binding has been shown to be dependent on pH and ionic strength, indicating its electrostatic nature (47). Indeed, similar to anionic lipids, the adsorption of Aβ on silica surfaces is pH dependent: ~90% at pH 7 and 4, whereas no adsorption was measured for pH 4, hence confirming that

the interaction of Aβ with silica is electrostatically driven. Furthermore, it has been reported that proteins with large intrinsically disordered regions are enriched in nanoparticle-adsorbed proteomes (48) attributed to the flexibility endowed by intrinsically disordered regions. Aβ oligomers have been shown to have similarly well-ordered β-sheet cores with intrinsically disordered termini (49). We expect the interaction between the disordered regions of Aβ aggregates and silica NBs to contribute to the tight binding observed herein.

There is a discrepancy that appears between NB-adsorbed Aβ in in vitro B103 cells, whereas that from buffer, of a total of 5 μM, NB adsorb $\sim$2.3 μM in cells but only 0.2 μM in buffer. This can be explained by the reasons that the distribution of Aβ species formed in buffer and cell culture system would be different in mass and structure, and NB have preference for one of the structures that has a higher population in cells than in solution. For example, heterogenous nucleation on membranes may lead to a different morphology of oligomers than nucleation in solution (26). mAβ does indeed have a higher population than ecAβ ($\sim$88 vs. $\sim$20%, Table 1), and indications are that NB's affinity for Aβ can be attributed to this specific oligomer structure.

A preference for a particular morphology is seen from size distributions derived from AFM and confocal microscopy after NB treatment (Figs. 1 *F* and 2 *F*). Both show a depletion of larger Aβ aggregates (height of 4 nm, area of 1 μm^2) after NB treatment and a relative increase in smaller aggregate sizes (2 nm height, 0.1 μm^2 area), suggesting a preference for relatively larger aggregates. Scavenging of larger aggregates eases the amyloid load in cell membranes, which is sufficient to reduce membrane leakage and increase cell viability. Smaller aggregates that are not scavenged can have implications for therapeutic applications. Small oligomers form toxic amyloid ion channels; however, their impact on cell viability in this study is minimal (lower dye leakage and increased cell viability), indicating that scavenging of amyloid aggregates significantly lowers the amyloid load and number of active amyloid channels (31,37). Moreover, because optical microscopy images are limited in resolution, we cannot rule out that these "small oligomers" are indeed aggregates or just monomers. Because the smaller aggregates can grow in size and become toxic to membranes over the course of time, repeated application of NB would be essential to scavenge toxic amyloids.

Nanoparticles have been previously used for scavenging amyloidogenic proteins from cells and animal models. For example, cerium oxide nanoparticles bind to α-synuclein in yeast cell plasma membranes, and magnetite nanoparticles functionalized with an Aβ antibody can remove it from animals using a method similar to dialysis (50,51). In fact, antibody-functionalized mesoporous silica nanoparticles have been shown to bind Aβ monomers and clear them from circulation (12). Antibody-modified nanoparticles will certainly have more specificity for Aβ monomers than NB. However, in contrast to these systems, we show that NB prefer a certain aggregate size and toxic species. This poses a unique advantage that monomeric forms of the protein will not be scavenged, allowing physiological functions to continue unaffected.

Applications for isolating toxic Aβ species from biological samples

In this work, we demonstrated that a simple vortexing step can be used to elute aggregates isolated by NB (Fig. 4 *A*). This addresses the challenges posed by traditional elution methods in which extreme pHs and harsh detergent conditions easily disrupt weakly held species. To demonstrate the applications of NB for diagnostics, we first sought to delineate the seeding capability of mAβ and ecAβ. Using ThT assays, it was found that they show distinct aggregation kinetics (Fig. 5 *C*). This supports the possibility of the presence of two distinct species that are spatially and temporally separated. In vivo evidence for two species of Aβ with distinct neurotoxicity was first proposed by Liu et al. (52) and has since been confirmed by many other studies (23,25). We show that NB scavenge amyloid aggregates in a time-resolved manner. At short NB incubation times, ecAβ is scavenged, whereas at longer incubation times, mAβ is sequestered (Fig. 4, *B* and *C*).

To use NB-scavenged Aβ for downstream characterization of Aβ aggregates isolated from cells and tissues, two critical questions arise: is the native structure and functional form of Aβ aggregates conserved and stable 1) upon NB binding and 2) after elution from the NB surface? We observed that mAβ dissociate from cell membranes to re-equilibrate ecAβ levels (Table 1), indicating that mAβ has conformational flexibility to form hydrogen bonds with water. This is consistent with previous reports that soluble oligomeric Aβ is capable of binding to membranes, implying stability of mAβ in both aqueous and lipid environments (7,53,54).

Results described above suggest the likelihood that mAβ retain several native structural features once bound to NB's hydrophilic silica surface. NB-Aβ indeed show elongation rates comparable to mAβ (Fig. 5 *C*), confirming the conservation of aggregation driving domains of native structure. Stability after desorption is confirmed as desorbed NB-Aβ shows identical ThT binding characteristics as when adsorbed (Fig. 5 *C*). These results allow us to propose an alternative workflow to isolate Aβ species from cell and tissue environments, using NB as shown in Fig. S3. This approach will provide an opportunity to study a more comprehensive ensemble of transient and detergent soluble species formed during the aggregation cascade in vivo.

CONCLUSIONS

We have designed silica nanobowls that have high affinity for Aβ because of their anionic surface. NB are covered

with a lipid-polymer coating that regulates protein adsorption and cell interactions. These NB, when incubated with neuroblasts containing Aβ in their plasma membrane, rescue Aβ pathology as shown by mitochondrial metabolic activity and dye leakage from cells. Protein quantification reveals that ∼75% of Aβ is adsorbed on NB. Hence, the therapeutic effect of NB has been attributed to their ability to scavenge Aβ. By seeding NB-associated Aβ into a monomer solution, we determined that Aβ fractions are scavenged in a time-resolved manner. The adsorption of Aβ on NB is shown to be reversible by mechanical agitation and Aβ aggregation is unaffected by NB. Seeding experiments confirmed that the structure of the aggregation driving domain of Aβ aggregates are conserved during scavenging and desorption. Scavenging with NB is a unique and powerful approach to remove amyloid aggregates from cells, tissues, and circulating body fluids, reducing their toxic load as well as allowing for biophysical mechanistic study of their pathophysiology.

SUPPORTING MATERIAL

Supporting material can be found online at https://doi.org/10.1016/j.bpj.2021.07.002.

AUTHOR CONTRIBUTIONS

V.S. and R.L. designed the study and experiments. V.S., A.G.K., P.C., and M.S. conducted experiments and analyzed data. V.S., M.S., and R.L. wrote the manuscript.

ACKNOWLEDGMENTS

We thank Dr. D. Schubert (Salk Institute) for providing us with B103 cell line and Dr. P. Kyriakakis (University of California, San Diego (UCSD)) for Bradford and bicinchoninic acid assay reagents. We also thank Dr. L. Antonschmidt (Max Planck Institute for Biophysical Chemistry) for discussions about lipid assembly on surfaces, small molecule encapsulation, and protein interactions and N. Khosla (Eidgenössische Technische Hochschule Zürich)) and Dr. S. Ramachandran (UCSD) for helpful discussions on protein-cell interactions and biological applications. We would also like to thank the following core services: the UCSD Neuroscience Core (National Institutes of Health grant NS047101) and UCSD Electron Microscopy Facility and Timo Meerloo for TEM assistance.

This project was supported by the National Institute on Aging of National Institutes of Health (grant AG028709).

SUPPORTING CITATIONS

References (55–62) appear in the Supporting material.

REFERENCES

1. Selkoe, D. J., and J. Hardy. 2016. The amyloid hypothesis of Alzheimer's disease at 25 years. *EMBO Mol. Med.* 8:595–608.
2. Nguyen, P. H., A. Ramamoorthy, …, P. Derreumaux. 2021. Amyloid oligomers: a joint experimental/computational perspective on Alzheimer's disease, Parkinson's disease, type II diabetes, and amyotrophic lateral sclerosis. *Chem. Rev.* 4:2545–2647.
3. Sciacca, M. F. M., S. A. Kotler, …, A. Ramamoorthy. 2012. Two-step mechanism of membrane disruption by Aβ through membrane fragmentation and pore formation. *Biophys. J.* 103:702–710.
4. Jang, H., L. Connelly, …, R. Nussinov. 2013. Mechanisms for the insertion of toxic, fibril-like β-amyloid oligomers into the membrane. *J. Chem. Theory Comput.* 9:822–833.
5. Arispe, N., E. Rojas, and H. B. Pollard. 1993. Alzheimer disease amyloid beta protein forms calcium channels in bilayer membranes: blockade by tromethamine and aluminum. *Proc. Natl. Acad. Sci. USA.* 90:567–571.
6. Di Scala, C., N. Yahi, …, J. Fantini. 2016. Common molecular mechanism of amyloid pore formation by Alzheimer's β-amyloid peptide and α-synuclein. *Sci. Rep.* 6:28781.
7. Demuro, A., E. Mina, …, C. G. Glabe. 2005. Calcium dysregulation and membrane disruption as a ubiquitous neurotoxic mechanism of soluble amyloid oligomers. *J. Biol. Chem.* 280:17294–17300.
8. Brambilla, D., R. Verpillot, …, K. Andrieux. 2012. PEGylated nanoparticles bind to and alter amyloid-beta peptide conformation: toward engineering of functional nanomedicines for Alzheimer's disease. *ACS Nano.* 6:5897–5908.
9. Wu, W.-H., X. Sun, …, Y.-M. Li. 2008. TiO2 nanoparticles promote beta-amyloid fibrillation in vitro. *Biochem. Biophys. Res. Commun.* 373:315–318.
10. Bu, T., T. Zako, …, M. Maeda. 2015. Adsorption and separation of amyloid beta aggregates using ferromagnetic nanoparticles coated with charged polymer brushes. *J. Mater. Chem. B Mater. Biol. Med.* 3:3351–3357.
11. Cabaleiro-Lago, C., F. Quinlan-Pluck, …, S. Linse. 2010. Dual effect of amino modified polystyrene nanoparticles on amyloid β protein fibrillation. *ACS Chem. Neurosci.* 1:279–287.
12. Jung, H., Y. J. Chung, …, J. Lee. 2020. Silica nanodepletors: targeting and clearing Alzheimer's β-amyloid plaques. *Adv. Funct. Mater.* 30:1910475.
13. Arce, F. T., H. Jang, …, R. Lal. 2011. Polymorphism of amyloid β peptide in different environments: implications for membrane insertion and pore formation. *Soft Matter.* 7:5267–5273.
14. Luo, Q., Y.-X. Lin, …, H. Wang. 2018. A self-destructive nanosweeper that captures and clears amyloid β-peptides. *Nat. Commun.* 9:1802.
15. Giacomelli, C. E., and W. Norde. 2005. Conformational changes of the amyloid beta-peptide (1-40) adsorbed on solid surfaces. *Macromol. Biosci.* 5:401–407.
16. Williams, T. L., and L. C. Serpell. 2011. Membrane and surface interactions of Alzheimer's Aβ peptide–insights into the mechanism of cytotoxicity. *FEBS J.* 278:3905–3917.
17. Gobbi, M., F. Re, …, M. E. Masserini. 2010. Lipid-based nanoparticles with high binding affinity for amyloid-β1-42 peptide. *Biomaterials.* 31:6519–6529.
18. Bhowmik, D., K. R. Mote, …, S. Maiti. 2015. Cell-membrane-mimicking lipid-coated nanoparticles confer Raman enhancement to membrane proteins and reveal membrane-attached amyloid-β conformation. *ACS Nano.* 9:9070–9077.
19. Serra-Batiste, M., M. Ninot-Pedrosa, …, N. Carulla. 2016. Aβ42 assembles into specific β-barrel pore-forming oligomers in membrane-mimicking environments. *Proc. Natl. Acad. Sci. USA.* 113:10866–10871.
20. Jana, M. K., R. Cappai, …, G. D. Ciccotosto. 2016. Membrane-bound tetramer and trimer Aβ oligomeric species correlate with toxicity towards cultured neurons. *J. Neurochem.* 136:594–608.
21. Jan, A., D. M. Hartley, and H. A. Lashuel. 2010. Preparation and characterization of toxic Abeta aggregates for structural and functional studies in Alzheimer's disease research. *Nat. Protoc.* 5:1186–1209.
22. Kotler, S. A., J. R. Brender, …, A. Ramamoorthy. 2015. High-resolution NMR characterization of low abundance oligomers of amyloid-β without purification. *Sci. Rep.* 5:11811.

23. Lesné, S., M. T. Koh, …, K. H. Ashe. 2006. A specific amyloid-β protein assembly in the brain impairs memory. *Nature.* 440:352–357.

24. Jin, M., N. Shepardson, …, D. J. Selkoe. 2011. Soluble amyloid β-protein dimers isolated from Alzheimer cortex directly induce Tau hyperphosphorylation and neuritic degeneration. *Proc. Natl. Acad. Sci. USA.* 108:5819–5824.

25. Yang, T., S. Li, …, D. J. Selkoe. 2017. Large soluble oligomers of amyloid β-protein from alzheimer brain are far less neuroactive than the smaller oligomers to which they dissociate. *J. Neurosci.* 37:152–163.

26. Kotler, S. A., P. Walsh, …, A. Ramamoorthy. 2014. Differences between amyloid-β aggregation in solution and on the membrane: insights into elucidation of the mechanistic details of Alzheimer's disease. *Chem. Soc. Rev.* 43:6692–6700.

27. Cohen, M., B. Appleby, and J. G. Safar. 2016. Distinct prion-like strains of amyloid beta implicated in phenotypic diversity of Alzheimer's disease. *Prion.* 10:9–17.

28. Mo, A. H., P. B. Landon, …, R. Lal. 2016. Magnetically-responsive silica-gold nanobowls for targeted delivery and SERS-based sensing. *Nanoscale.* 8:11840–11850.

29. Zhang, Y., J. Cai, …, W. Xue. 2016. Effects of thermosensitive poly(N-isopropylacrylamide) on blood coagulation. *J. Mater. Chem. B Mater. Biol. Med.* 4:3733–3749.

30. Xue, C., N. Yonet-Tanyeri, …, D. E. Leckband. 2011. Protein adsorption on poly(N-isopropylacrylamide) brushes: dependence on grafting density and chain collapse. *Langmuir.* 27:8810–8818.

31. Lin, H., R. Bhatia, and R. Lal. 2019. Amyloid protein forms ion channels: implications for Alzheimer's disease pathophysiology.

32. Byrd, T. F., IV, L. T. Hoang, …, K. T. Seale. 2014. The microfluidic multitrap nanophysiometer for hematologic cancer cell characterization reveals temporal sensitivity of the calcein-AM efflux assay. *Sci. Rep.* 4:5117.

33. Becker, K., X. Wang, …, J. Ma. 2018. Detecting alpha synuclein seeding activity in formaldehyde-fixed MSA patient tissue by PMCA. *Mol. Neurobiol.* 55:8728–8737.

34. Colby, D. W., Q. Zhang, …, S. B. Prusiner. 2007. Prion detection by an amyloid seeding assay. *Proc. Natl. Acad. Sci. USA.* 104:20914–20919.

35. Orlando, A., E. Cazzaniga, …, F. Re. 2017. Mesoporous silica nanoparticles trigger mitophagy in endothelial cells and perturb neuronal network activity in a size- and time-dependent manner. *Int. J. Nanomedicine.* 12:3547–3559.

36. Nielsen, L., R. Khurana, …, A. L. Fink. 2001. Effect of environmental factors on the kinetics of insulin fibril formation: elucidation of the molecular mechanism. *Biochemistry.* 40:6036–6046.

37. Lee, J., Y. H. Kim, …, R. Lal. 2017. Amyloid β ion channels in a membrane comprising brain total lipid extracts. *ACS Chem. Neurosci.* 8:1348–1357.

38. Lambert, M. P., A. K. Barlow, …, W. L. Klein. 1998. Diffusible, nonfibrillar ligands derived from Abeta1-42 are potent central nervous system neurotoxins. *Proc. Natl. Acad. Sci. USA.* 95:6448–6453.

39. Watanabe-Nakayama, T., K. Ono, …, M. Yamada. 2016. High-speed atomic force microscopy reveals structural dynamics of amyloid β1-42 aggregates. *Proc. Natl. Acad. Sci. USA.* 113:5835–5840.

40. Tsolakis, A. C., E. Halevas, …, G. Litsardakis. 2017. Magnetic fluorescent nanoparticles binding to amyloid-beta peptide: silica-coated, thioflavin-T functionalized iron oxide. *IEEE Trans. Magn.* 53:1–4.

41. Chauhan, A., I. Ray, and V. P. S. Chauhan. 2000. Interaction of amyloid beta-protein with anionic phospholipids: possible involvement of Lys28 and C-terminus aliphatic amino acids. *Neurochem. Res.* 25:423–429.

42. Valdes-Gonzalez, T., J. Inagawa, and T. Ido. 2001. Neuropeptides interact with glycolipid receptors: a surface plasmon resonance study. *Peptides.* 22:1099–1106.

43. Williams, T. L., B. R. G. Johnson, …, L. C. Serpell. 2011. Aβ42 oligomers, but not fibrils, simultaneously bind to and cause damage to ganglioside-containing lipid membranes. *Biochem. J.* 439:67–77.

44. Som, M., R. Lal, and V. Ruiz-Velasco. 2020. Lipid-encapsulated silica nanobowls as an efficient and versatile DNA delivery system. *Bioconjug. Chem.* 31:2697–2711.

45. Bouchoucha, M., É. Béliveau, …, M. A. Fortin. 2017. Antibody-conjugated mesoporous silica nanoparticles for brain microvessel endothelial cell targeting. *J. Mater. Chem. B Mater. Biol. Med.* 5:7721–7735.

46. Kremer, J. J., and R. M. Murphy. 2003. Kinetics of adsorption of β-amyloid peptide Abeta(1-40) to lipid bilayers. *J. Biochem. Biophys. Methods.* 57:159–169.

47. Ikeda, K., and K. Matsuzaki. 2008. Driving force of binding of amyloid β-protein to lipid bilayers. *Biochem. Biophys. Res. Commun.* 370:525–529.

48. Romashchenko, A. V., T. W. Kan, …, Y. M. Moshkin. 2017. Nanoparticles associate with intrinsically disordered RNA-binding proteins. *ACS Nano.* 11:1328–1339.

49. Ciudad, S., E. Puig, …, N. Carulla. 2020. Aβ(1–42) tetramer and octamer structures reveal edge conductivity pores as a mechanism for membrane damage. *Nat. Commun.* 11:3014.

50. Ruotolo, R., G. De Giorgio, …, N. Marmiroli. 2020. Cerium oxide nanoparticles rescue α-synuclein-induced toxicity in a yeast model of Parkinson's disease. *Nanomaterials (Basel).* 10:235.

51. Kim, D., H. J. Kwon, and T. Hyeon. 2019. Magnetite/ceria nanoparticle assemblies for extracorporeal cleansing of amyloid-β in Alzheimer's disease. *Adv. Mater.* 31:e1807965.

52. Liu, P., M. N. Reed, …, K. H. Ashe. 2015. Quaternary structure defines a large class of amyloid-β oligomers neutralized by sequestration. *Cell Rep.* 11:1760–1771.

53. Valincius, G., F. Heinrich, …, M. Lösche. 2008. Soluble amyloid β-oligomers affect dielectric membrane properties by bilayer insertion and domain formation: implications for cell toxicity. *Biophys. J.* 95:4845–4861.

54. Kayed, R., Y. Sokolov, …, C. G. Glabe. 2004. Permeabilization of lipid bilayers is a common conformation-dependent activity of soluble amyloid oligomers in protein misfolding diseases. *J. Biol. Chem.* 279:46363–46366.

55. Schubert, D., S. Heinemann, …, B. L. Brandt. 1974. Clonal cell lines from the rat central nervous system. *Nature.* 249:224–227.

56. Chaput, D., L. H. Kirouac, …, J. Padmanabhan. 2012. SILAC-based proteomic analysis to investigate the impact of amyloid precursor protein expression in neuronal-like B103 cells. *Electrophoresis.* 33:3728–3737.

57. Nhan, H. S., K. Chiang, and E. H. Koo. 2015. The multifaceted nature of amyloid precursor protein and its proteolytic fragments: friends and foes. *Acta Neuropathol.* 129:1–19.

58. Schubert, D., and C. Behl. 1993. The expression of amyloid beta protein precursor protects nerve cells from β-amyloid and glutamate toxicity and alters their interaction with the extracellular matrix. *Brain Res.* 629:275–282.

59. De Felice, F. G., D. Wu, …, W. L. Klein. 2008. Alzheimer's disease-type neuronal tau hyperphosphorylation induced by A beta oligomers. *Neurobiol. Aging.* 29:1334–1347.

60. Kirouac, L., A. J. Rajic, …, J. Padmanabhan. 2017. Activation of Ras-ERK signaling and GSK-3 by amyloid precursor protein and amyloid beta facilitates neurodegeneration in Alzheimer's disease. *eNeuro.* 4:ENEURO.0149-16.2017.

61. Chung, C. W., Y. H. Song, …, Y. K. Jung. 2001. Proapoptotic effects of Tau cleavage product generated by caspase-3. *Neurobiol. Dis.* 8:162–172.

62. Wang, Z. X., L. Tan, …, J. T. Yu. 2016. The essential role of soluble Aβ oligomers in Alzheimer's disease. *Mol. Neurobiol.* 53:1905–1924.